Acoustic characterization of echogenic liposomes: Frequency-dependent attenuation and backscatter

Jonathan A. Kopechek[a)]
Department of Biomedical Engineering, University of Cincinnati, 2901 Campus Drive, Cincinnati, Ohio 45221

Kevin J. Haworth
Department of Internal Medicine, Division of Cardiovascular Diseases, University of Cincinnati, 231 Albert B. Sabin Way, Cincinnati, Ohio 45267

Jason L. Raymond, T. Douglas Mast, and Stephen R. Perrin, Jr.
Department of Biomedical Engineering, University of Cincinnati, 2901 Campus Drive, Cincinnati, Ohio 45221

Melvin E. Klegerman and Shaoling Huang
Department of Internal Medicine, Division of Cardiology, University of Texas Health Science Center at Houston, Houston, Texas 77030

Tyrone M. Porter
Department of Mechanical Engineering, Boston University, 110 Cummington Street, Boston, Massachusetts 02215

David D. McPherson
Department of Internal Medicine, Division of Cardiology, University of Texas Health Science Center at Houston, Houston Texas 77030

Christy K. Holland
Department of Internal Medicine, Division of Cardiovascular Diseases, University of Cincinnati, 231 Albert B. Sabin Way, Cincinnati, Ohio 45267

(Received 19 October 2010; revised 18 January 2011; accepted 19 January 2011)

Ultrasound contrast agents (UCAs) are used clinically to aid detection and diagnosis of abnormal blood flow or perfusion. Characterization of UCAs can aid in the optimization of ultrasound parameters for enhanced image contrast. In this study echogenic liposomes (ELIPs) were characterized acoustically by measuring the frequency-dependent attenuation and backscatter coefficients at frequencies between 3 and 30 MHz using a broadband pulse-echo technique. The experimental methods were initially validated by comparing the attenuation and backscatter coefficients measured from 50-μm and 100-μm polystyrene microspheres with theoretical values. The size distribution of the ELIPs was measured and found to be polydisperse, ranging in size from 40 nm to 6 μm in diameter, with the highest number observed at 65 nm. The ELIP attenuation coefficients ranged from 3.7 ± 1.0 to 8.0 ± 3.3 dB/cm between 3 and 25 MHz. The backscatter coefficients were 0.011 ± 0.006 (cm str)$^{-1}$ between 6 and 9 MHz and 0.023 ± 0.006 (cm str)$^{-1}$ between 13 and 30 MHz. The measured scattering-to-attenuation ratio ranged from 8% to 22% between 6 and 25 MHz. Thus ELIPs can provide enhanced contrast over a broad range of frequencies and the scattering properties are suitable for various ultrasound imaging applications including diagnostic and intravascular ultrasound. © *2011 Acoustical Society of America*. [DOI: 10.1121/1.3626124]

PACS number(s): 43.80.Gx, 43.80.Vj [CCC] Pages: 3472–3481

I. INTRODUCTION

Traditional means to identify and treat arterial disease are hampered by an inability to localize atheroma extent and composition.[1] Since first examined by Bangham *et al*.,[2] liposomes have been developed for a wide range of technical and medical applications. Echogenic liposomes (ELIPs), which are phospholipid bilayer vesicles enclosing gas and fluid, are being developed as targeted echo contrast agents to permit evaluation of vasoactive and pathologic endothelium.[3,4] Echogenic liposomal dispersions are prepared by dispersing lipids in water, adding mannitol, and freeze-drying, or lyophilizing, and finally rehydrating.[5–7] The echogenicity of these preparations is due to the presence of gas, which is entrapped and stabilized by the lipid during the rehydration process.[8]

ELIPs can be targeted to certain tissues by attaching specific ligands and antibodies to the surface of liposomes.[9,10] For example, ELIPs coupled to anti-VCAM-1 antibodies highlight pathologic endothelium at early stages of atherosclerosis development.[4] Similarly, the linkage of a liposome with inactivated tissue plasminogen activator can identify and highlight thrombus or plaque rupture.[11] Lanza *et al*. have also demonstrated that a multistep biotinylated, lipid-coated,

[a)]Author to whom correspondence should be addressed. Electronic mail: jonathan.kopechek@gmail.com

perfluorocarbon nanoemulsion could be successfully targeted to thrombi *in vivo* while maintaining ultrasound contrast.[12] These authors have additionally demonstrated that this ultrasound agent can infiltrate arterial walls and localize tissue factor expression.[13] Unger *et al*. created targeted microbubbles containing perfluorobutane that were approximately 2 μm and were able to bind to thrombus *in vitro*.[14,15]

Ultrasound contrast agents (UCAs) are effective for diagnostic purposes when they provide greater contrast than the surrounding tissues. The UCA size and shell properties and the ultrasound insonation parameters affect the amount of contrast produced.[16,17] Acoustic characterization of UCA properties entails measuring the frequency-dependent attenuation and backscatter coefficients.[18,19] The frequency-dependent scattering-to-attenuation ratio (STAR), a normalized continuous value between 0 and 1 for omnidirectional scatterers, can be determined from these measurements. Attenuation of ultrasound due to absorption by UCAs, which decreases the STAR value, can cause shadowing artifacts and reduce contrast distal to blood vessels. Thus a STAR value of 100%, where attenuation is due entirely to scattering and no energy is absorbed, is ideal for imaging.[20,21]

Ultrasound contrast agents differ primarily in size, shell material, and gas content. Most commercially available contrast agents have a mean diameter between 1 and 5 μm and consist of microbubbles encapsulated with an albumin, polymer, or lipid shell. Many ultrasound contrast agents contain inert heavy gases, such as sulfur hexafluoride or perfluorocarbons, which have low solubility in water and thus increase the lifetime of the microbubbles in circulation.[16,22] ELIPs can contain air or a bioactive gas such as nitric oxide or xenon and have a mean diameter of less than 1 μm.[23–25] Compared with commercially available UCAs, the difference in ELIP size, shell composition, and gas content may impact the frequency-dependent attenuation and backscatter coefficients. Consequently, the insonation parameters for imaging ELIPs in diagnostic ultrasound applications may be significantly different.

The objective of this study was to characterize ELIPs acoustically by measuring the frequency-dependent attenuation and backscatter coefficients using a broadband approach. The experimental methods used for characterizing ELIPs were first validated by measuring the attenuation and backscatter coefficients of polystyrene microspheres and comparing the results to theoretical values.[26,27] In addition, the size distribution of ELIPs was measured in order to provide an estimate of the encapsulated bubble size distribution. This study will reveal the ultrasound frequencies between 3 and 30 MHz over which ELIPs scatter efficiently. The attenuation and backscatter results will aid in choosing optimal frequencies for ELIP imaging.

II. MATERIALS AND METHODS

A. Preparation of echogenic liposomes

Standard preparations of liposomes were received in individual vials (6 mg lipid/vial, lyophilized) from the University of Texas Health Science Center in Houston and formulated as previously described.[8] Stock suspensions were made by adding 0.6 ml of air-saturated, 0.2-μm filtered deionized water at room temperature (20–24 °C) to each vial of lyophilized lipid, yielding ELIPs with a lipid concentration of 10 mg/ml. To maximize the entrapment of air within the liposomes, the 0.2-μm filtered, deionized water was stored in a air-pressurized chamber at 200 kPa above atmospheric pressure for up to four hours to obtain a dissolved oxygen concentration of 9.5 ± 0.25 mg/L. A dissolved oxygen meter was used for all dissolved oxygen concentration measurements (DO 100 Series, Oakton, Vernon Hills, IL). The stock suspension was diluted in a bovine serum albumin (BSA) solution (0.5% albumin wt./vol. in phosphate-buffered saline) to a final lipid concentration of 0.05 mg/ml, which has been used previously for *in vivo* experiments.[28] The albumin solution was observed to reduce aggregation and coalescence of ELIP during the experiment.

B. Size distribution measurements

The size distribution of ELIPs in 0.5% BSA was measured using two instruments: a Multisizer 3 fitted with a 20-μm aperture tube (Beckman-Coulter, Miami, FL) and a Zetasizer Nano ZS (Malvern, Worcestershire, UK). The Multisizer 3 measures changes in electrical impedance to count particles with equivalent spherical diameters between 2% and 40% of the intake aperture. The Zetasizer employs dynamic light scattering to determine the size distribution of particles and was used to measure the size distribution of ELIP below 0.46 μm in diameter. Due to the size resolution limitations of the Multisizer 3, the two distributions were concatenated at 450 nm to determine the entire ELIP size distribution. Both techniques have been used previously to size liposomes and ultrasound contrast agents.[19,29–36]

Transmission electron micrograph (TEM) images of ELIPs were acquired for comparison. ELIPs were reconstituted in water at a concentration of 1 mg/ml and negatively stained using 1% uranyl acetate on 300 mesh formvar carbon grids (EMS, Hatfield, PA). Negative-stained ELIP samples were imaged at 60 kV with a Gatan Bioscan 792 CCD camera (Pleasanton, CA) on a JEOL 1200 transmission electron microscope (Tokyo, Japan).

C. Transducer characterization

Calibration and mapping of the acoustic field was conducted in a 36 in. × 24 in. × 20 in. acrylic tank filled with 0.2-μm filtered, deionized water with a dissolved oxygen concentration of 3.0 ± 0.5 mg/L. All pressure measurements were made with a 0.2-mm PVDF needle hydrophone (Precision Acoustics, Ltd., Dorchester, UK). A motorized three-axis orthogonal translation system (Velmex NF90 Series, Velmex, Inc., Bloomfield, NY) was used to step the hydrophone throughout the acoustic field. The calibration system was automated and controlled using MATLAB software (Mathworks, Natick, MA). The hydrophone signal was acquired using a digital oscilloscope (WaveRunner-2 LT572, LeCroy, Chestnut Ridge, NY) and transferred to a PC for analysis using MATLAB.

D. Experimental setup

A diagram of the experimental setup is provided in Fig. 1. Broadband attenuation and backscatter measurements were

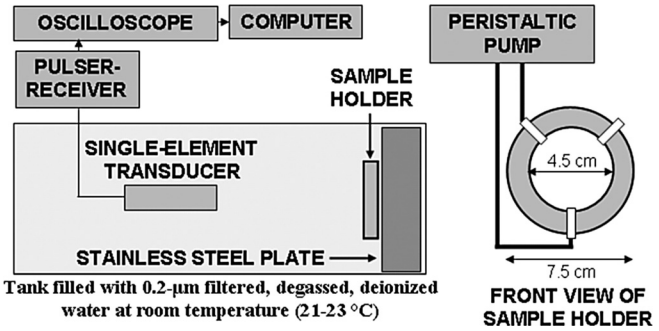

FIG. 1. A schematic of the experimental setup. Single-element transducers were driven with a pulser-receiver and the received echoes were displayed on an oscilloscope and acquired using MATLAB. A custom-built sample holder was constructed by boring a 4.5-cm hole into the center of a 0.6-cm thick circular PVC disk. Three ports were drilled into the side of the disk for filling and draining the sample chamber using a peristaltic pump. The front and back of the sample holder were covered with latex sheets.

conducted in a 17 in. × 9 in. × 9 in. acrylic tank filled with 0.2-μm filtered, deionized water at room temperature (22 ± 1 °C) with a dissolved oxygen concentration of 3.0 ± 0.5 mg/L. A custom-built sample chamber was constructed from a 0.6-cm thick circular PVC disk with an outer diameter of 7.5 cm. A circular 4.5-cm hole was bored into the center of the disk and three ports were drilled into the side of the disk, each separated by approximately 120°, for filling and draining the sample chamber. The front and back of the sample chamber were covered with latex (Durex, Norcross, GA) with a thickness of less than 0.2 mm. The acoustic impedance of latex is similar to water, resulting in a reflection coefficient less than 0.2. A precision-ground, stainless steel plate (1 in. ± 0.002 in. thick, type 316, McMaster-Carr ETC) was placed directly behind the sample chamber as an acoustic reflector for attenuation measurements. The sample chamber was centered at the focus of the transducer, or the Rayleigh distance (position of peak pressure amplitude) for unfocused transducers.

An ultrasound pulser-receiver (UTA-3, Aerotech Laboratories, Pittsburgh, PA) was used to generate the excitation pulse and amplify the received ultrasound signal. The input voltage to the transducer was controlled with an in-line 50-Ohm attenuator (SA-50, Texscan, Indianapolis, IN). A custom-built transmit/receive switch was used to separate the transmitted signals from the received signals. The received signals were amplified and time-gated with the UTA-3, digitized (8 bits, 100 MHz sampling rate) using an oscilloscope (WaveRunner-2 LT572, LeCroy, Chestnut Ridge, NY), and transferred to a PC for analysis with MATLAB. For each attenuation and backscatter measurement 1000 waveforms were acquired, the power spectrum was computed for each waveform, and the 1000 power spectra were averaged. Reference measurements (i.e., reflections from the stainless steel plate) were also acquired before adding the polystyrene spheres or ELIPs to the solution.

Five single-element transducers were used for this study in order to characterize ELIPs across a range of frequencies from 3 to 30 MHz: two unfocused transducers for attenuation measurements and three focused transducers for backscatter measurements (Olympus-NDT, Waltham, MA). Unfocused transducers provided better bandwidth for attenuation measurements but poor signal-to-noise for backscatter measurements compared with focused transducers. The characteristics of each transducer are listed in Table I. The input pulse to each transducer was a negative voltage spike less than 20 ns in duration with a pulse repetition frequency of 350 Hz, thus a broadband method could be used to measure the attenuation or backscatter coefficients simultaneously over a range of frequencies. The usable bandwidth of each transducer was determined by the frequency range where the signal-to-noise ratio was greater than 6 dB, where the noise level was measured without scatterers present. The peak-to-peak pressure for all measurements was 33 kPa, which was the lowest pressure that could be used to obtain a signal-to-noise ratio greater than 6 dB for all transducers while avoiding acoustically driven diffusion and rapid framentation.[37–39] Examples of the transmitted signal from the focused 15-MHz transducer and received signal from ELIP backscatter are shown in Fig. 2.

E. Data analysis

In order to determine the frequency-dependent attenuation coefficient, 1000 echoes returning from the stainless steel plate were acquired with and without polystyrene spheres or ELIPs in the sample holder and power spectra were computed for each acquired pulse. The attenuation coefficient in decibels per unit length, $\alpha_{\mathrm{dB}}(f)$, was calculated as a function of frequency, f, using the following equation:

$$\alpha_{dB}(f) = \frac{10\log_{10}\left(\frac{\langle|S_r(f)|\rangle}{\langle|S_s(f)|\rangle}\right)}{x}, \quad (1)$$

where $\langle|S_s(f)|\rangle$ and $\langle|S_r(f)|\rangle$ are the average power spectrum with and without scatterers, respectively, and x is the acoustic path length within the sample.[40] To determine the frequency-dependent backscatter coefficient, 1000 signals were acquired over a 3.33-μs time-gated region within the sample chamber and the power spectra were computed for each

TABLE I. Transducer characteristics for attenuation and backscatter measurements.

Transducer model number	Center frequency (MHz)	Aperture diameter (mm)	Focal distance (cm)	−3 dB beamwidth (mm)
Panametrics V313 (unfocused)	15.0	6	9.0[a]	2.0
Panametrics V356 (unfocused)	30.0	6	6.0[a]	3.0
Panametrics V320 (focused)	7.5	13	4.7	1.0
Harisonic I31504P (focused)	15.0	6	3.6	1.0
Harisonic HI-988 (focused)	30.0	6	1.9	0.2

[a]Rayleigh distance for unfocused transducers.

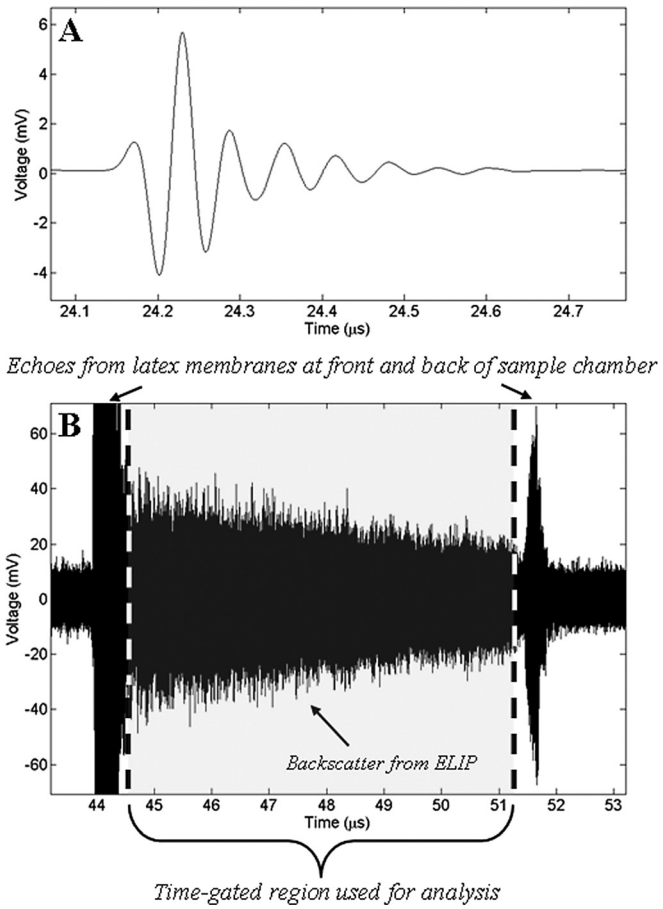

FIG. 2. (A) Time-domain signal transmitted by the focused Harisonic 15-MHz transducer and acquired using a 0.2-mm PVDF needle hydrophone. (B) An example of the time-domain backscatter signals received with a focused Harisonic 15-MHz transducer at a peak pressure of 33 kPa. The echoes from the latex membranes at the front and back of the sample chamber are shown and scattering from ELIP is evident inside the sample chamber. The dashed lines highlight the time-gated portion (shaded) of the signal used to compute the power spectra.

time-gated signal. The backscatter coefficient, $\eta(f)$, was computed using the following equation:

$$\eta(f) = \frac{\left\langle |V_s(f)|^2 \right\rangle}{\left\langle |V_r(f)|^2 \right\rangle} \frac{X(f)}{A_s(f)}, \tag{2}$$

where $\langle |V_s(f)|^2 \rangle$ is the average power spectrum magnitude of the time-gated backscattered signal, which was normalized by the average reference backscattered power spectrum magnitude, $\langle |V_r(f)|^2 \rangle$, obtained in a separate measurement where the stainless steel reflector plate was placed at the same distance as the center of the sample chamber.[41] $A_s(f)$ and $X(f)$ are attenuation compensation and diffraction correction factors, respectively, for broadband measurements. The attenuation compensation factor, $A_s(f)$, developed by Sigelmann and Reid[18] is given in the following form by Marsh *et al.*:[41]

$$A_s(f) = e^{(-4\alpha_A(f)x_0)} \cdot e^{(-2\alpha_A(f)l)} \cdot \frac{e^{(2\alpha_A(f)l)} - e^{(-2\alpha_A(f)l)}}{4\alpha_A(f)l}, \tag{3}$$

where $\alpha_A(f)$ is the measured amplitude attenuation coefficient (converted to units of Np/cm), x_0 is the distance between the front surface of the sample and the front of the time-gated region within the sample, and l is the physical length of the time-gated region within the sample.[41] The transducer diffraction correction factor, $X(f)$, for a spherically focused transducer is given by Chen *et al.*:[42]

$$X(f) = \frac{r_0^2}{l\pi a^2 E_\infty} \cdot e^{\left(-2/\sqrt{\pi G_p}\right)}, \tag{4}$$

where r_0 is the focal distance, l is the physical length of the time-gated region, a is the transducer aperture radius, E_∞ is the ratio between the effective and geometrical beam cross-sections of the transducer (a constant value of 0.46), and G_p is the pressure gain factor defined as $ka^2/2r_0$.[42] The frequency-dependent scattering-to-attenuation ratio, STAR(f), is defined as

$$\mathrm{STAR}(f) = \frac{10}{\log(10)} \cdot \frac{4\pi \cdot \eta(f)}{\alpha_{dB}(f)}, \tag{5}$$

where $\alpha_{\mathrm{dB}}(f)$ and $\eta(f)$ are the attenuation and backscatter coefficients defined using Eqs. (1) and (2).[20,43]

F. Experimental and theoretical attenuation and backscatter of elastic microspheres

The frequency-dependent attenuation and backscatter coefficients of 50-μm and 100-μm polystyrene microspheres (4K-50μm and 4K100, Duke Scientific, Palo Alto, CA) were measured to validate the accuracy of the experimental techniques and diffraction corrections applied to all measurements. The microspheres were diluted in Isoton II solution (Beckman Coulter, Miami, FL), and the suspension was circulated at a flow rate of 20 ml/min using a peristaltic pump (Masterflex, Cole-Parmer, Chicago, IL) to prevent the microspheres from settling to the bottom of the sample chamber. The size distributions were taken to be Gaussian distributions using the standard deviations provided by the manufacturer (1.0% and 1.5% for the 50-μm and 100-μm spheres, respectively). The number densities of microspheres in each suspension were measured using a Coulter Counter Z1 (Beckman Coulter, Miami, FL). For theoretical computations the size distribution was subdivided into 21 equally spaced bins ranging from diameters of 48.5–51.5 μm and 95–105 μm for the 50-μm and 100-μm spheres, respectively.

The results were compared to theoretical values for the attenuation and backscatter coefficients of solid elastic spheres.[26,27,44,45] The theoretical attenuation coefficient was computed based on the work of Faran[26] and Hall *et al.*:[27]

$$\alpha_{dB}(f) = \sum_m \left(n(a_m) \frac{2\pi}{k^2} \sum_{q=0}^{q_{\max}} (2q+1) \left| A_{q,m} \right|^2 \right), \tag{6}$$

where m indexes bins corresponding to microspheres of radius a_m, $n(a_m)$ is the number density of microspheres of radius a_m, and k is the wavenumber outside the scatterer corresponding to frequency, f. $A_{q,m}$ is the amplitude of scattered partial waves defined by Hay and Schaafsma,[45] q indexes

over the spherical Bessel function order used in computing $A_{q,m}$, and $q_{\max}$ is the highest order spherical Bessel function used, which was set to 15 because higher orders were found to be negligible at all frequencies.

The theoretical backscatter coefficient, $\eta(f)$, is defined as

$$\eta(f) = \sum_m n(a_m) \left. \frac{d\sigma_m}{d\Omega} \right|_{\Omega=180^\circ}, \tag{7}$$

where $n(a_m)$ is the number density defined in Eq. (6) and $d\sigma_m/d\Omega|_{\Omega=180^\circ}$ is the differential backscatter cross section for a microsphere of radius a_m.[27] The differential backscatter cross section is defined as

$$\left. \frac{d\sigma_m}{d\Omega} \right|_{\Omega=180^\circ} = (r_{\text{scat}}^2) \frac{I_{\text{scat}}(r, \theta = 180^\circ)}{I_{\text{inc}}}, \tag{8}$$

where r_{scat} is the distance from the scatterer to the observation point, I_{scat} is the intensity measured at the observation point, which is assumed to be far from the scatterer location and 180° from the direction of insonation, and I_{inc} is the insonation intensity.[46] Far from the scatterer ($kr_{\text{scat}} \gg 1$) the scattered intensity can be written as

$$I_{\text{scat}} = a_m \frac{I_{\text{inc}}}{(2r_{\text{scat}})^2} |f_\infty|^2, \tag{9}$$

where a_m and r_{scat} are defined in Eqs. (7) and (8), respectively, and f_∞ is the backscatter form factor given by Hay and Mercer:[47]

$$f_\infty = -\frac{2}{ka_m} \sum_{q=0}^{q_{\max}} (2q+1)(-1)^q i A_{q,m}, \tag{10}$$

where $A_{q,m}$ is defined in Eq. (6). Combining Eqs. (7)–(10), the backscatter coefficient, $\eta(f)$, can be computed from the expression:

$$\eta(f) = \sum_m \left(n(a_m) \cdot \left| \frac{-i}{k} \sum_{q=0}^{q_{\max}} (2q+1)(-1)^q A_{q,m} \right|^2 \right) \tag{11}$$

with the variables defined in Eq. (6). The densities inside and outside the scatterer were set to 1.055 and 1.000 g/mL, respectively, and the compressional velocities inside and outside the scatterer were 2380 and 1490 m/s, respectively, obtained from the literature.[27] A shear velocity of 1120 m/s (Poisson ratio of 0.3578) provided the best agreement with the experimental results and is within the range of previously published values.[45,48,49] Attenuative losses within each polystyrene scatterer were ignored.

G. Theoretical attenuation and backscatter coefficients of encapsulated bubbles

A computational model was implemented in MATLAB to determine the theoretical attenuation and backscatter coefficients of ELIP for comparison to the experimental measurements. The theory is based on Church's model for encapsulated bubble dynamics, which gives the scattering cross section, σ_s, and damping terms as a function of the bubble size, shell, gas and surrounding liquid parameters.[50] Using the scattering cross section from Church's model, the theoretical attenuation coefficient can be determined, as given by Goertz *et al.*:[51]

$$\alpha_t(f) = \frac{10}{\log(10)} \sum_r n(r) \sigma_s(r,f) \frac{\delta_{\text{tot}}(r,f)}{\delta_{\text{rad}}(r,f)}, \tag{12}$$

where $n(r)$ is the number density of bubbles of radius r,[51] and σ_s, δ_{tot}, and δ_{rad} are the scattering cross section, total damping, and acoustic radiation damping terms, respectively, computed using Church's model. The theoretical backscatter coefficient, $\eta_t(f)$, is given by Marsh *et al.*:[41]

$$\eta_t(f) = \frac{\sum_r n(r) \sigma_s(r,f)}{4\pi}, \tag{13}$$

where $n(r)$ and σ_s are defined in Eq. (12).[41] The size distribution was divided into 2400 bins with each bin spaced 1.4 nm apart. The number density of the ELIPs was on the order of 10^6 in each bin below a diameter of 70 nm and on the order of 10^3 in each bin under 1.12 μm. The unknown variables in the theoretical model were the size distribution of ELIP bubbles, the shell shear modulus, and the shell shear viscosity. The ELIP size distribution was measured experimentally and the unknown shell parameters were estimated by fitting the theory to the measured attenuation and backscatter coefficients. A least-squares minimization fit was used to determine the shell parameter values and the ratio of encapsulated gas volume relative to the liposome volume, which was assumed to be constant for all ELIPs regardless of size. ELIPs were assumed to be spherical and encapsulate a single spherical gas bubble surrounded by a monolayer shell of thickness 1.5 nm.[52]

III. RESULTS

A. ELIP size distribution

The size distribution of ELIP vesicles is shown in Fig. 3, plotted by number density and percent by volume, assuming ELIPs are spherical in shape. ELIPs have a polydisperse distribution and range from 40 nm to 6 μm in diameter. The largest number density was observed at a diameter of 65 nm. At a concentration of 0.05 mg/ml, the total number density was 6.37×10^8 liposomes/ml.

B. Attenuation and backscatter coefficients of elastic microspheres

The frequency-dependent attenuation and backscatter coefficients of polystyrene microspheres are shown in Figs. 4 and 5, respectively. The theoretical coefficients are also plotted for comparison. The correlation coefficient between experiment and theory was 0.98 for the attenuation coefficients and 0.87 for the backscatter coefficients, thus there was very good agreement between the experimental and theoretical values for each elastic spheres measurement.

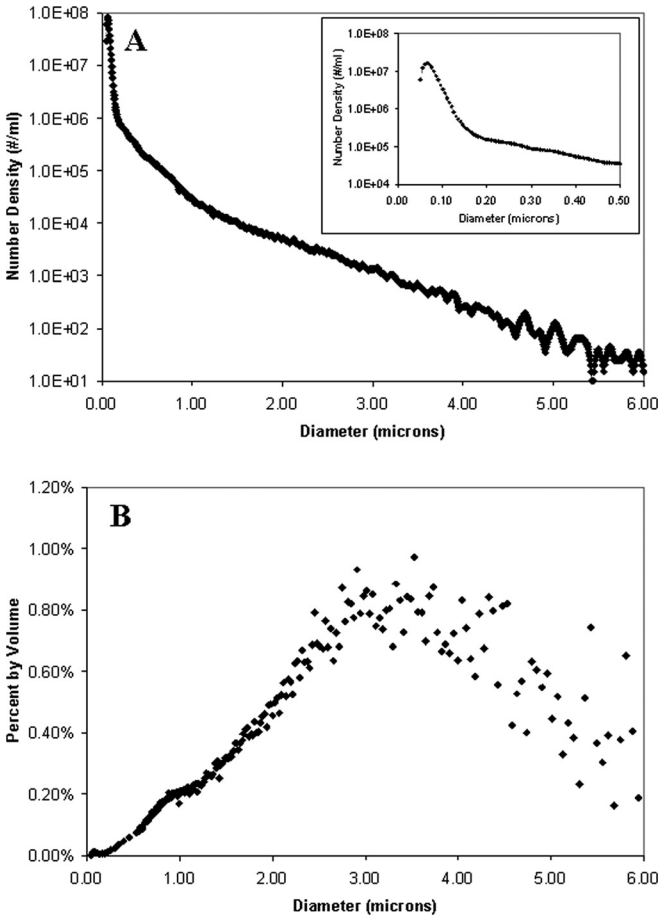

FIG. 3. The size distribution of ELIP vesicles (A) by number and (B) by volume (assuming spherical vesicles), determined by concatenating results from a Malvern Zetasizer Nano ZS and a Coulter Multisizer 3. The inset plot in (A) highlights the peak at 65 nm.

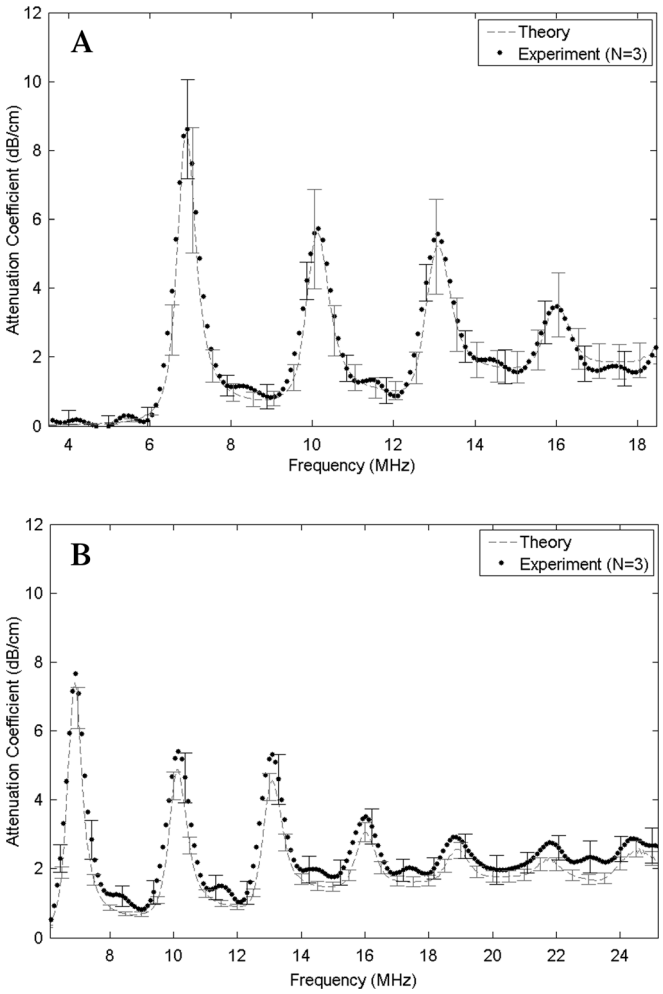

FIG. 4. The frequency-dependent attenuation coefficient of polystyrene microspheres compared with theory using three single-element broadband transducers at a peak output pressure of 33 kPa. (A) A 15-MHz unfocused transducer with 100-μm polystyrene microspheres (number density of 3040 ± 805 microspheres/ml) and (B) a 30-MHz unfocused transducer with 100-μm polystyrene microspheres (number density of 2636 ± 236 microspheres/ml). Representative error bars shown on some of the experimental data represent mean $\pm$ standard deviation of the measured attenuation coefficients for three measurements. Error bars on the theoretical values represent the uncertainty of the theory due to the standard deviation of the microsphere number density measurements.

C. Attenuation and backscatter coefficients of ELIPs

The frequency-dependent attenuation and backscatter coefficients of ELIPs are shown in Figs. 6 and 7, respectively. Theoretical values from the computational model are also plotted for comparison. In addition, the experimental and theoretical scattering-to-attenuation ratios are shown in Fig. 8. The best fit between theoretical and experimental values was achieved by assuming a shell thickness of 1.5 nm,[52] a shell shear modulus of 125 MPa, a shell shear viscosity of 0.3 Pa s, and that the gas bubble occupies 18% of the ELIP volume. Using these parameters the peak attenuation and backscatter coefficients occurred at 13 MHz but decreased by only 3 dB between 7 and 30 MHz. Also, these parameters resulted in STAR values ranging from 14 to 17% between 5 and 25 MHz, compared with measured STAR values of 8%–22%.

IV. DISCUSSION

The frequency-dependent attenuation and backscatter coefficients of echogenic liposomes have been determined and elucidate that ELIPs can be used across a broad range of frequencies for imaging. The broadband pulse-echo experimental technique was validated by measuring the coefficients for polystyrene microspheres and comparing them to theoretical values.[27,41] In our study there was very good agreement between the experimental and theoretical values below 20 MHz, and the measurement uncertainties were comparable to previously published studies.[27,45,53] The divergence of the theory from experimental values above 20 MHz is likely due to attenuative losses within each polystyrene microsphere, which were ignored in the theoretical treatment.[26,27] These results confirm the validity of the broadband pulse-echo experimental techniques used to measure attenuation and backscatter in this study.

The frequency-dependent attenuation and backscatter coefficients of ELIPs have not been measured previously using a broadband approach. However, other ultrasound contrast agents have been characterized acoustically using this approach. The resonance frequencies of Albunex, Definity, Levovist, Sonazoid, and polymer-encapsulated air bubbles were observed at frequencies between 2 and 10 MHz, as

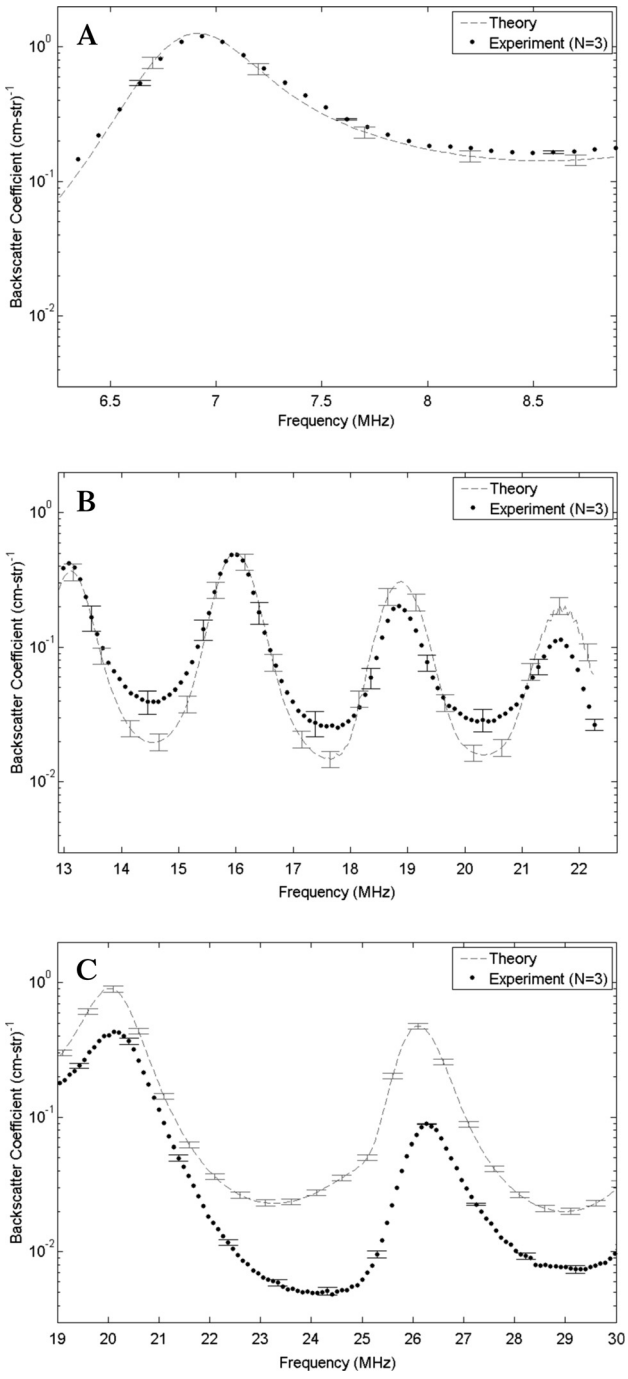

FIG. 5. The frequency-dependent backscatter coefficient of polystyrene microspheres compared with theory using three single-element broadband transducers at a peak output pressure of 33 kPa. (A) A 7.5-MHz focused transducer with 100-μm polystyrene microspheres (number density of 4840 $\pm$ 457 microspheres/ml), (B) a 15-MHz focused transducer with 100-μm polystyrene microspheres (number density of 3948 $\pm$ 556 microspheres/ml), and (C) a 30-MHz focused transducer with 50-μm polystyrene microspheres (number density of 16 600 $\pm$ 815 microspheres/ml). Representative error bars shown on some of the experimental data represent mean $\pm$ standard deviation of the measured backscatter coefficients for three measurements. Error bars on the theoretical values represent the uncertainty of the theory due to the standard deviation of five microsphere number density measurements.

predicted for most encapsulated bubbles larger than 1 μm in diameter.[20,51,54–56] However, the results of this study indicate the ELIP scatter efficiently across a broad range of frequencies due to the polydisperse size distribution.

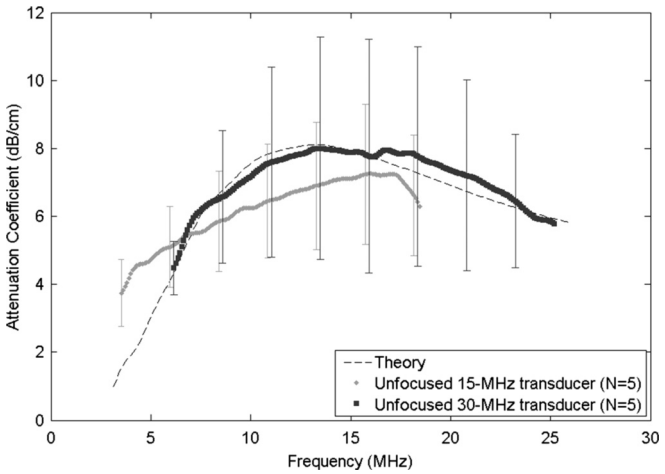

FIG. 6. The measured frequency-dependent attenuation coefficient of ELIP and theory, based on a fit to the data, using two single-element broadband transducers at a peak output pressure of 33 kPa. Error bars represent the standard deviation of the measured attenuation coefficients for five ELIP samples.

Many ultrasound contrast agents, including Definity, Sonazoid, and Sonovue, have relatively monodisperse bubble populations above 1 μm in diameter.[51,55,57] However, the size distribution of ELIPs is much more polydisperse, ranging from 40 nm to 6 μm in diameter. As a result of the polydisperse bubble population, the STAR, attenuation and backscatter coefficients do not change significantly (less than 3 dB) between 7 and 25 MHz. This suggests that ELIP may be used for applications across a broad range of frequencies, including intravascular ultrasound (20 MHz or higher) and also diagnostic imaging.

The measured scattering-to-attenuation ratio varied from 8% to 22%, which is within the range of other UCAs studied previously, including Levovist (2%–12%) and Albunex (5%–60%).[20,43] The shear elastic moduli of Definity, Albunex, and Sonazoid have been found to be 190, 89, and 52 MPa, respectively, while the shell shear viscosities were

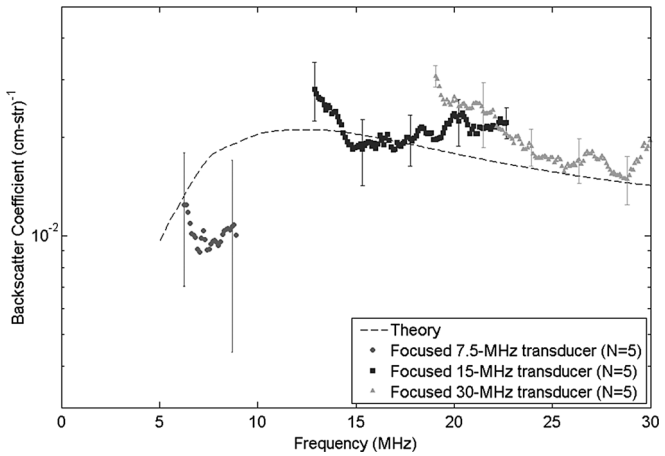

FIG. 7. The measured frequency-dependent backscatter coefficient of ELIP and theory, based on a fit to the measured data, using three single-element broadband transducers at a peak output pressure of 33 kPa. Error bars represent the standard deviation of the measured backscatter coefficients for five ELIP samples.

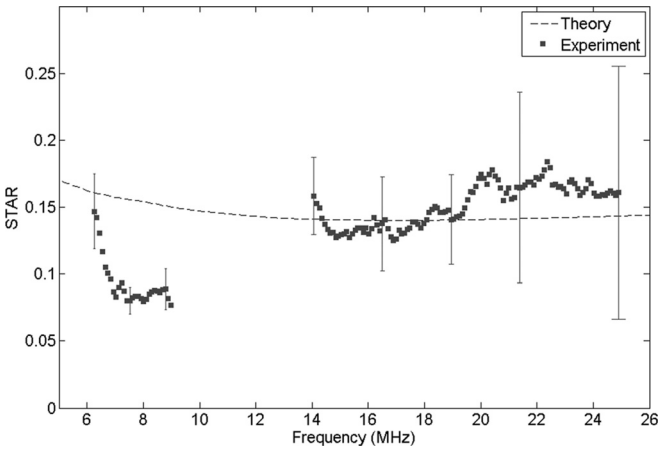

FIG. 8. The frequency-dependent scattering-to-attenuation ratio (STAR) of ELIP compared with theory, based on the overlapping data between Figs. 6 and 7. Error bars represent propagated uncertainty of the five attenuation and five backscatter measurements.

found to be 0.07, 1.77, and 0.99 Pa s, respectively.[50,51,54,55] Thus, the shear elastic modulus and shell shear viscosity of ELIP determined in this study, 125 MPa and 0.30 Pa s, respectively, are within the range of other contrast agents.

A limitation of the computational model used in this study was the inability to directly measure the bubble sizes within ELIP. Instead, the bubble sizes were indirectly assumed to be 18% of the liposome volume (which was measured directly). This value resulted in the best fit between experimental results and theory, and is within the range of 10%–33% that has previously been reported.[23,58] A transmission electron micrograph (TEM) image of ELIPs is shown in Fig. 9. ELIPs with a bilayer shell can be identified and individual bubbles encapsulated by a monolayer shell are visible. Although some broad assumptions were made, the results of this study suggest that the computational model is useful for estimating the shell properties of ELIPs by using the attenuation and backscatter coefficients measured experimentally.

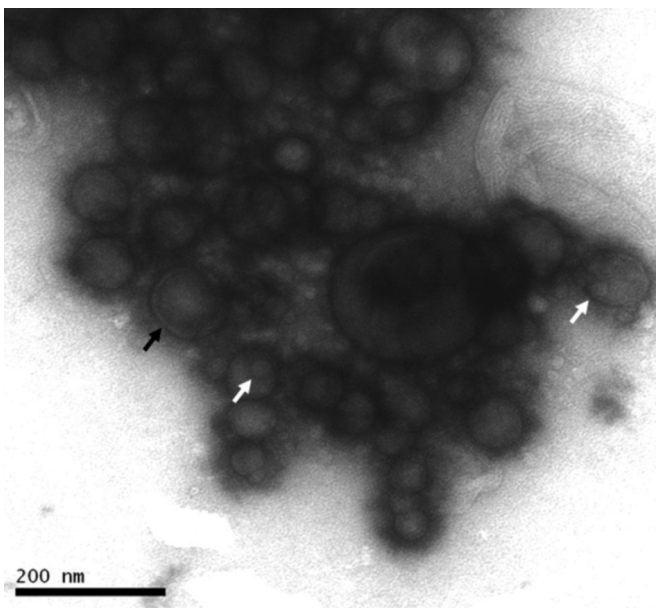

FIG. 9. Transmission electron micrograph of negative-stained ELIP revealing a broad range of sizes (150k × magnification). The white arrows indicate encapsulated bubbles within a lipid monolayer while the black arrow indicates a phospholipid bilayer.

Several ultrasound contrast agents, including Definity, Sonazoid, Optison, and Sonovue, have been used to nucleate cavitation.[59–62] Cavitation has been associated with enhanced thrombolysis, sonoporation, drug release, and drug delivery across the blood-brain barrier.[63–66] ELIPs have also been investigated as a cavitation nucleation agent in addition to their role as a diagnostic ultrasound contrast agents.[67,68] Although nonlinear bubble oscillations were not examined in this study, the results indicate that ELIPs may be able to nucleate cavitation across a broad range of frequencies due to their broad size distribution. Thus drug-loaded ELIPs may be effective in various therapeutic applications, including ultrasound-enhanced thrombolysis and ultrasound-mediated drug delivery.[69–72]

V. CONCLUSIONS

The frequency-dependent attenuation and backscatter coefficients of ELIPs have been measured. The results of this study suggest that ELIPs can be used for applications across a broad range of frequencies including intravascular and diagnostic ultrasound imaging. These results will aid in choosing appropriate acoustic parameters for future ELIP imaging applications.

ACKNOWLEDGMENTS

We thank Giovanni M. Pauletti, Ph.D., for providing access to the Malvern Zetasizer and Joel Mobley, Ph.D., for the use of the focused 7.5-MHz transducer. This work was supported by two grants from the National Institutes of Health, Grant Nos. NIH R01 HL059586, NIH R01 HL74002, and NIH R01 NS047603.

[1]S. Vaina and C. Stefanadis, "Detection of the vulnerable coronary atheromatous plaque. Where are we now?," Int. J. Cardiovasc. Intervent. **7**, 75–87 (2005).
[2]A. D. Bangham, M. M. Standish, and J. C. Watkins, "Diffusion of univalent ions across the lamellae of swollen phospholipids," J. Mol. Biol. **13**, 238–252 (1965).
[3]S. M. Demos, H. Alkan-Onyuksel, B. J. Kane, K. Ramani, A. Nagaraj, R. Greene, M. Klegerman, and D. D. McPherson, "In vivo targeting of acoustically reflective liposomes for intravascular and transvascular ultrasonic enhancement," J. Am. Coll. Cardiol. **33**, 867–875 (1999).
[4]A. J. Hamilton, S. L. Huang, D. Warnick, M. Rabbat, B. Kane, A. Nagaraj, M. Klegerman, and D. D. McPherson, "Intravascular ultrasound molecular imaging of atheroma components in vivo," J. Am. Coll. Cardiol. **43**, 453–460 (2004).
[5]H. Alkan-Onyuksel, S. M. Demos, G. M. Lanza, M. J. Vonesh, M. E. Klegerman, B. J. Kane, J. Kuszak, and D. D. McPherson, "Development of inherently echogenic liposomes as an ultrasonic contrast agent," J. Pharm. Sci. **85**, 486–490 (1996).
[6]H. Alkan-Onyuksel, S. M. Demos, B. Kane, D. D. Mcpherson, and R. C. MacDonald, "Echogenic immunoliposomes as an ultrasound imaging agent," in *ICAST Proceedings* (1996), pp. 40–47.
[7]S. L. Huang, A. J. Hamilton, A. Nagaraj, S. D. Tiukinhoy, M. E. Klegerman, D. D. McPherson, and R. C. Macdonald, "Improving ultrasound reflectivity and stability of echogenic liposomal dispersions for use as targeted ultrasound contrast agents," J. Pharm. Sci. **90**, 1917–1926 (2001).
[8]S. L. Huang, A. J. Hamilton, E. Pozharski, A. Nagaraj, M. E. Klegerman, D. D. McPherson, and R. C. MacDonald, "Physical correlates of the

ultrasonic reflectivity of lipid dispersions suitable as diagnostic contrast agents," Ultrasound Med. Biol. **28**, 339–348 (2002).
[9]F. J. Martin and T. D. Heath, "Covalent attachment of proteins to liposomes," in *Liposomes: A Practical Approach*, edited by N. RRC (IRL Press, New York, 1990), Chap. 4.
[10]J. P. Leonetti, P. Machy, G. Degols, B. Lebleu and L. Leserman, "Antibody-targeted liposomes containing oligodeoxyribonucleotides complementary to viral RNA selectively inhibit viral replication," Proc. Natl. Acad. Sci. U.S.A. **87**, 2448–2451 (1990).
[11]M. E. Klegerman, Y. Zou, and D. D. McPherson, "Fibrin targeting of echogenic liposomes with inactivated tissue plasminogen activator," J. Liposome Res. **18**, 95–112 (2008).
[12]G. M. Lanza, K. D. Wallace, M. J. Scott, W. P. Cacheris, D. R. Abendschein, D. H. Christy, A. M. Sharkey, J. G. Miller, P. J. Gaffney, and S. A. Wickline, "A novel site-targeted ultrasonic contrast agent with broad biomedical application," Circulation **94**, 3334–3340 (1996).
[13]G. M. Lanza, D. R. Abendschein, C. S. Hall, M. J. Scott, D. E. Scherrer, A. Houseman, J. G. Miller, and S. A. Wickline, "In vivo molecular imaging of stretch-induced tissue factor in carotid arteries with ligand-targeted nanoparticles," J. Am. Soc. Echocardiogr. **13**, 608–614 (2000).
[14]E. C. Unger, P. J. Lund, D. K. Shen, T. A. Fritz, D. Yellowhair, and T. E. New, "Nitrogen-filled liposomes as a vascular US contrast agent: Preliminary evaluation," Radiology **185**, 453–456 (1992).
[15]E. C. Unger, T. P. McCreery, R. H. Sweitzer, D. Shen, and G. Wu, "In vitro studies of a new thrombus-specific ultrasound contrast agent," Am. J. Cardiol. **81**, 58G–61G (1998).
[16]N. de Jong, M. Emmer, A. van Wamel, and M. Versluis, "Ultrasonic characterization of ultrasound contrast agents," Med. Biol. Eng. Comput. **47**, 861–873 (2009).
[17]C. X. Deng and F. L. Lizzi, "A review of physical phenomena associated with ultrasonic contrast agents and illustrative clinical applications," Ultrasound Med. Biol. **28**, 277–286 (2002).
[18]R. A. Sigelman and J. A. Reid, "Analysis and measurement of ultrasound backscattering from an ensemble of scatterers excited by sine-wave bursts," J. Acoust. Soc. Am. **53**, 1351–1355 (1973).
[19]L. Hoff, *Acoustic Characterization of Contrast Agents for Medical Ultrasound Imaging* (Kluwer Academic Publishers, Norwell, MA, 2001), pp. 89–141.
[20]A. Bouakaz, N. De Jong, and C. Cachard, "Standard properties of ultrasound contrast agents," Ultrasound Med. Biol. **24**, 469–472 (1998).
[21]P. J. Frinking and N. de Jong, "Acoustic modeling of shell-encapsulated gas bubbles," Ultrasound Med. Biol. **24**, 523–533 (1998).
[22]S. Kaul, "Myocardial contrast echocardiography: a 25-year retrospective," Circulation **118**, 291–308 (2008).
[23]S. L. Huang, D. D. McPherson, and R. C. Macdonald, "A method to co-encapsulate gas and drugs in liposomes for ultrasound-controlled drug delivery," Ultrasound Med. Biol. **34**, 1272–1280 (2008).
[24]S. L. Huang, P. H. Kee, H. Kim, M. R. Moody, S. M. Chrzanowski, R. C. Macdonald, and D. D. McPherson, "Nitric oxide-loaded echogenic liposomes for nitric oxide delivery and inhibition of intimal hyperplasia," J. Am. Coll. Cardiol. **54**, 652–659 (2009).
[25]G. L. Britton, H. Kim, P. H. Kee, J. Aronowski, C. K. Holland, D. D. McPherson, and S. L. Huang, "In vivo therapeutic gas delivery for neuroprotection with echogenic liposomes," Circulation **122**, 1578–1587 (2010).
[26]J. J. Faran, Jr., "Sound Scattering by Solid Cylinders and Spheres," J. Acoust. Soc. Am. **23**, 405–418 (1951).
[27]C. S. Hall, J. N. Marsh, M. S. Hughes, J. Mobley, K. D. Wallace, J. G. Miller, and G. H. Brandenburger, "Broadband measurements of the attenuation coefficient and backscatter coefficient for suspensions: A potential calibration tool," J. Acoust. Soc. Am. **101**, 1162–1171 (1997).
[28]A. Hamilton, S. L. Huang, D. Warnick, A. Stein, M. Rabbat, T. Madhav, B. Kane, A. Nagaraj, M. Klegerman, R. MacDonald, and D. McPherson, "Left ventricular thrombus enhancement after intravenous injection of echogenic immunoliposomes: Studies in a new experimental model," Circulation **105**, 2772–2778 (2002).
[29]I. Buttino, G. De Rosa, Y. Carotenuto, A. Ianora, A. Fontana, F. Quaglia, M. I. La Rotonda, and A. Miralto, "Giant liposomes as delivery system for ecophysiological studies in copepods," J. Exp. Bio. **209**, 801–809 (2006).
[30]J. Guan and T. J. Matula, "Using light scattering to measure the response of individual ultrasound contrast microbubbles subjected to pulsed ultrasound *in vitro*," J. Acoust. Soc. Am. **116**, 2832–2842 (2004).
[31]M. E. Klegerman, M. Wassler, S. L. Huang, Y. Zou, H. Kim, H. S. Shelat, C. K. Holland, Y. J. Geng, and D. D. McPherson, "Liposomal modular complexes for simultaneous targeted delivery of bioactive gases and therapeutics," J. Control. Release **142**, 326–331 (2010).
[32]G. Korpanty, S. Chen, R. V. Shohet, J. Ding, B. Yang, P. A. Frenkel, and P. A. Grayburn, "Targeting of VEGF-mediated angiogenesis to rat myocardium using ultrasonic destruction of microbubbles," Gene Therapy **12**, 1305–1312 (2005).
[33]J. Kotynska and Z. A. Figaszewski, "Adsorption equilibria between liposome membrane formed of phosphatidylcholine and aqueous sodium chloride solution as a function of pH," Biochim. Biophys. Acta **1720**, 22–27 (2006).
[34]H. Takeuchi, Y. Matsui, H. Yamamoto, and Y. Kawashima, "Mucoadhesive properties of carbopol or chitosan-coated liposomes and their effectiveness in the oral administration of calcitonin to rats," J. Control. Release **86**, 235–242 (2003).
[35]Z. Xing, H. Ke, J. Wang, B. Zhao, X. Yue, Z. Dai and J. Liu, "Novel ultrasound contrast agent based on microbubbles generated from surfactant mixtures of Span 60 and polyoxyethylene 40 stearate," Acta Biomater. **6**, 3542–3549 (2010).
[36]K. D. Buchanan, S. Huang, H. Kim, R. C. Macdonald, and D. D. McPherson, "Echogenic liposome compositions for increased retention of ultrasound reflectivity at physiologic temperature," J. Pharm. Sci. **97**, 2242–2249 (2008).
[37]A. Bouakaz, M. Versluis, and N. de Jong, "High-speed optical observations of contrast agent destruction," Ultrasound Med. Biol. **31**, 391–399 (2005).
[38]D. A. Smith, T. M. Porter, J. Martinez, S. Huang, R. C. MacDonald, D. D. McPherson, and C. K. Holland, "Destruction thresholds of echogenic liposomes with clinical diagnostic ultrasound," Ultrasound Med. Biol. **33**, 797–809 (2007).
[39]J. E. Chomas, P. Dayton, J. Allen, K. Morgan, and K. W. Ferrara, "Mechanisms of contrast agent destruction," IEEE Trans. Ultrason. Ferroelectr. Freq. Control **48**, 232–248 (2001).
[40]C. C. Coussios, C. K. Holland, L. Jakubowska, S. L. Huang, R. C. MacDonald, A. Nagaraj, and D. D. McPherson, "In vitro characterization of liposomes and Optison by acoustic scattering at 3.5 MHz," Ultrasound Med. Biol. **30**, 181–190 (2004).
[41]J. N. Marsh, M. S. Hughes, C. S. Hall, S. H. Lewis, R. L. Trousil, H. Levene, and J. G. Miller, "Frequency and concentration dependence of the backscatter coefficient of the ultrasound contrast agent Albunex," J. Acoust. Soc. Am. **104**, 1654–1666 (1998).
[42]X. Chen, D. Phillips, K. Q. Schwarz, J. G. Mottley, and K. J. Parker, "The measurement of backscatter coefficient from a broadband pulse-echo system: a new formulation," IEEE Trans. Ultrason. Ferroelectr. Freq. Control **44**, 515–525 (1997).
[43]J. N. Marsh, M. S. Hughes, G. H. Brandenburger, and J. G. Miller, "Broadband measurement of the scattering-to-attenuation ratio for Albunex at 37 degrees C," Ultrasound Med. Biol. **25**, 1321–1324 (1999).
[44]R. Hickling, "Analysis of echoes from a solid elastic sphere in water," J. Acoust. Soc. Am. **34**, 1582–1592 (1962).
[45]A. E. Hay and A. S. Schaafsma, "Resonance scattering in suspensions," J. Acoust. Soc. Am. **85**, 1124–1138 (1989).
[46]A. D. Pierce, *Acoustics: An Introduction to its Physical Principles and Applications* (Acoustical Society of America, Melville, NY, 1989), p. 428.
[47]A. E. Hay and D. G. Mercer, "On the theory of sound scattering and viscous absorption in aqueous suspensions at medium and short wavelengths," J. Acoust. Soc. Am. **78**, 1761–1771 (1985).
[48]D. S. Hughes, E. B. Blankenship, and R. L. Mims, "Variation of elastic moduli and wave velocity with pressure and temperature in plastics," J. Appl. Phys. **21**, 294–297 (1950).
[49]J. A. Rinde, "Poisson's ratio for rigid plastic foams," J. Appl. Polym. Sci. **14**, 1913–1926 (1970).
[50]C. C. Church, "The effects of an elastic solid surface layer on the radial pulsations of gas bubbles," J. Acoust. Soc. Am. **97**, 1510–1521 (1995).
[51]D. E. Goertz, N. de Jong, and A. F. van der Steen, "Attenuation and size distribution measurements of Definity and manipulated Definity populations," Ultrasound Med. Biol. **33**, 1376–1388 (2007).
[52]J. Miñones, Jr., J. M. Rodríguez Patino, O. Conde, C. Carrera, and R. Seoane, "The effect of polar groups on structural characteristics of phospholipid monolayers spread at the air–water interface," Colloids Surf. A: Physicochem. Eng. Aspects **203**, 273–286 (2002).
[53]T. T. Jansson, T. D. Mast, and R. C. Waag, "Measurements of differential scattering cross section using a ring transducer," J. Acoust. Soc. Am. **103**, 3169–3179 (1998).

[54]N. de Jong and L. Hoff, "Ultrasound scattering properties of Albunex microspheres," Ultrasonics **31**, 175–181 (1993).
[55]K. Sarkar, W. T. Shi, D. Chatterjee, and F. Forsberg, "Characterization of ultrasound contrast microbubbles using in vitro experiments and viscous and viscoelastic interface models for encapsulation," J. Acoust. Soc. Am. **118**, 539–550 (2005).
[56]L. Hoff, P. C. Sontum and J. M. Hovem, "Oscillations of polymeric microbubbles: effect of the encapsulating shell," J. Acoust. Soc. Am. **107**, 2272–2280 (2000).
[57]C. Greis, "Technology overview: SonoVue (Bracco, Milan)," Eur. Radiol. **14**, 11–15 (2004).
[58]S. L. Huang and R. C. MacDonald, "Acoustically active liposomes for drug encapsulation and ultrasound-triggered release," Biochim. Biophys. Acta **1665**, 134–141 (2004).
[59]S. Datta, C. C. Coussios, A. Y. Ammi, T. D. Mast, G. M. de Courten-Myers, and C. K. Holland, "Ultrasound-enhanced thrombolysis using Definity as a cavitation nucleation agent," Ultrasound Med. Biol. **34**, 1421–1433 (2008).
[60]W. T. Shi, F. Forsberg, A. Tornes, J. Ostensen, and B. B. Goldberg, "Destruction of contrast microbubbles and the association with inertial cavitation," Ultrasound Med. Biol. **26**, 1009–1019 (2000).
[61]M. D. Santin, D. A. King, J. Foiret, A. Haak, W. D. O'Brien, Jr., and S. L. Bridal, "Encapsulated contrast microbubble radial oscillation associated with postexcitation pressure peaks," J. Acoust. Soc. Am. **127**, 1156–1164 (2010).
[62]K. E. Hitchcock and C. K. Holland, "Ultrasound-assisted thrombolysis for stroke therapy: Better thrombus break-up with bubbles," Stroke **41**, S50–S53 (2010).
[63]S. Datta, C. C. Coussios, L. E. McAdory, J. Tan, T. Porter, G. De Courten-Myers, and C. K. Holland, "Correlation of cavitation with ultrasound enhancement of thrombolysis," Ultrasound Med. Biol. **32**, 1257–1267 (2006).
[64]G. A. Husseini, M. A. Diaz de la Rosa, E. S. Richardson, D. A. Christensen, and W. G. Pitt, "The role of cavitation in acoustically activated drug delivery," J. Control. Release **107**, 253–261 (2005).
[65]N. McDannold, N. Vykhodtseva, and K. Hynynen, "Targeted disruption of the blood-brain barrier with focused ultrasound: Association with cavitation activity," Phys. Med. Biol. **51**, 793–807 (2006).
[66]Y. Zhou, J. Cui, and C. X. Deng, "Dynamics of sonoporation correlated with acoustic cavitation activities," Biophys. J. **94**, L51–L53 (2008).
[67]K. E. Hitchcock, D. N. Caudell, J. T. Sutton, M. E. Klegerman, D. Vela, G. J. Pyne-Geithman, T. Abruzzo, P. E. Cyr, Y. J. Geng, D. D. McPherson, and C. K. Holland, "Ultrasound-enhanced delivery of targeted echogenic liposomes in a novel ex vivo mouse aorta model," J. Control. Release **144**, 288–295 (2010).
[68]C. K. Holland and D. D. McPherson, "Echogenic Lipsomes for Targeted Drug Delivery," Proc. IEEE Int. Symp. Biomed. Imaging 2009, 755–758 (2009).
[69]G. J. Shaw, J. M. Meunier, S. L. Huang, C. J. Lindsell, D. D. McPherson, and C. K. Holland, "Ultrasound-enhanced thrombolysis with tPA-loaded echogenic liposomes," Thromb. Res. **124**(3), 306–310 (2009).
[70]D. A. Smith, S. S. Vaidya, J. A. Kopechek, S. L. Huang, M. E. Klegerman, D. D. McPherson, and C. K. Holland, "Ultrasound-triggered release of recombinant tissue-type plasminogen activator from echogenic liposomes," Ultrasound. Med. Biol. **36**, 145–157 (2010).
[71]J. A. Kopechek, T. M. Abruzzo, B. Wang, S. M. Chrzanowski, D. A. Smith, P. H. Kee, S. Huang, J. H. Collier, D. D. McPherson, and C. K. Holland, "Ultrasound-mediated release of hydrophilic and lipophilic agents from echogenic liposomes," J. Ultrasound. Med. **27**, 1597–1606 (2008).
[72]S. L. Huang, "Liposomes in ultrasonic drug and gene delivery," Adv. Drug Deliv. Rev. **60**, 1167–1176 (2008).